Interface magnetism and electronic structure: ZnO(0001)/Co_3O_4(111)

I. M. Kupchak,[1,*] N. F. Serpak,[1] A. Shkrebtii,[2] and R. Hayn[3]

[1]*V. Lashkarev Institute of Semiconductor Physics, NAS Ukraine, 45, Prospect Nauky, Kyiv 03680, Ukraine*

[2]*University of Ontario Institute of Technology, 2000 Simcoe Street North, Oshawa, Ontario, Canada L1H 7K4*

[3]*Aix-Marseille Université, CNRS, IM2NP-UMR 7334, 13397 Marseille Cedex 20, France*

(Received 26 April 2017; revised manuscript received 15 January 2018; published 14 March 2018)

We have studied the structural, electronic, and magnetic properties of spinel Co_3O_4(111) surfaces and their interfaces with ZnO(0001) using density functional theory within the generalized gradient approximation with the on-site Coulomb repulsion term. Two possible forms of spinel surface, containing Co^{2+} or Co^{3+} ions and terminated with either cobalt or oxygen ions, were considered, as well as their interface with zinc oxide. Our calculations demonstrate that Co^{3+} ions attain nonzero magnetic moments at the surface and interface, in contrast to the bulk, where they are not magnetic, leading to the ferromagnetic ordering. Since heavily Co doped ZnO samples can contain a Co_3O_4 secondary phase, such magnetic ordering at the interface might explain the origin of the magnetism in such diluted magnetic semiconductors.

DOI: 10.1103/PhysRevB.97.125304

I. INTRODUCTION

Magnetic semiconductors (MSs) and diluted magnetic semiconductors (DMSs) exhibit both ferromagnetic and semiconducting properties. Therefore, they are promising materials for spintronics, which utilizes not only the electron charge but also its spin for information processing. Historically, the first DMS with a high Curie temperature up to about 200 K was GaAs doped with Mn ions [1,2]. In that compound, the ferromagnetism is promoted by hole carriers, which align along the local Mn magnetic moments, and is called carrier-induced ferromagnetism or Zener *p-d* exchange. It is crucial for this mechanism that Mn at the Ga site becomes Mn^{2+} instead of Ga^{3+}, thus providing at the same time a local spin and a hole charge carrier. Extension of the mechanism proposed in a very influential paper [3] by Dietl and coworkers allows a prediction that the above room-temperature ferromagnetism in ZnO:Co and GaN:Mn is due to the same carrier-induced mechanism. The same carrier-induced mechanism would be responsible for the ferromagnetism with a sufficiently high number of hole charge carriers. The first experiments after that prediction [4] seemed to confirm the proposed mechanism, which was also supported by *ab initio* calculations [5]. However, it soon turned out that the Co impurity is, in fact, isovalent to the Zn ion [6] and provides no charge carriers at all, while the situation in GaN:Mn is similar [7].

We are going to concentrate here on ZnO:Co, for which the experimental reports demonstrate that the above room-temperature ferromagnetism in ZnO:Co persists. Even though its origin has still not been clarified, there are clear indications in more recent experiments that the magnetism in the ZnO:Co system can be attributed to the formation of the Co_3O_4 phase in ZnO [8–12]. Therefore, we will focus here on the role of the Co_3O_4 phase, although several attempts to explain the mechanism of the ferromagnetism in realistic ZnO:Co systems exist, including spinodal decomposition [13] and Lieb-Mattis ferrimagnetism [14], to cite just two ideas.

The typical doping level of Co in ZnO can be relatively high (in the range between 10% and 30%). This leads to the secondary phases of Co_3O_4 and $ZnCo_2O_4$ segregation during the sample growth, which can be detected, for instance, by Raman spectroscopy [12,15]. Although, in general, the appearance of such secondary phases is detrimental for DMS materials, this effect can also be advantageous. However, a lack of understanding of the secondary phases and their interfaces remains currently the main obstacle toward the practical applications of Co_3O_4 surfaces and their interfaces. By carrying out the first-principles simulations of the Co_3O_4/ZnO interface we not only offer realistic explanations to the big puzzle of the nature of ferromagnetism in DMS but also show the promise for new applications.

Cobalt oxide, Co_3O_4, also known as tricobalt tetraoxide or cobalt spinel, is a *p*-type semiconductor with a reported optical energy band gap E_g between 1.1 and 1.65 eV (see [16] and references therein). It is widely used in lithium-ion batteries as a cathode material [17], gas sensing, nanomaterials and nanojunctions, and environmental and numerous other applications [18–21]. Co_3O_4 crystallizes in the cubic normal spinel structure, which contains cobalt ions in two different oxidation states, Co^{2+} and Co^{3+}, located at the interstitial tetrahedral (A) and octahedral (B) sites, respectively (see, e.g., Ref. [16]). The bulk magnetic properties of the cobalt oxide are well understood. In the presence of a tetrahedral crystal field, the fivefold-degenerate atomic *d* orbitals of Co^{2+} ions are split into two groups, e_g and t_{2g}, leading to three unpaired *d* electrons on the t_{2g} orbital. Similarly, in the case of a Co^{3+} ion, the crystal field is octahedral, and the splitting leads to six paired electrons in the t_{2g} orbital, while the e_g orbital is empty. As a result, the Co^{2+} ions carry a permanent magnetic moment, whereas Co^{3+} ions are not magnetic. Considering only the A-site sublattice, each Co^{2+} ion is surrounded by

*kupchak@isp.kiev.ua

four neighbors with oppositely directed spin, thus forming an antiferromagnetic (AFM) state. In general, such a nearest A-A exchange interaction is expected to be weak since in typical spinel structures with magnetic cations, A-B coupling between the ions in tetrahedral and octahedral sites is dominant [22]. However, in the Co_3O_4 spinel this A-A coupling is unusually strong due to the indirect exchange through the intermediate Co^{3+} ions in the octahedral B site, providing Co^{2+} ions with a magnetic moment of about $3.02\mu_B$. As a result of such strong coupling, Co_3O_4 is antiferromagnetic below the Néel temperature $T_N \sim 40$ K and paramagnetic at higher temperatures [22].

When such a complex structure is terminated by a surface or forms an interface, one can expect new interesting magnetic peculiarities that are absent in the bulk of the crystal. Indeed, the formation of a surface or interface between different materials involves several important factors, such as surface polarity, charge transfer, stresses, and defects, altering the long-range magnetic ordering and the magnetic response as a result [23,24]. There are many publications on the electronic and magnetic properties of different spinels and their surfaces, such as the Fe_3O_4 spinel (see, e.g., [24]), which has a crystal structure similar to that of Co_3O_4. However, cobalt spinel surfaces are still not that well understood, and even more complex behavior should be expected when the interface with other materials is formed. It has been shown that during the epitaxial growth of Co_3O_4, two surfaces with the lowest surface energy, namely, (111) and (110), are typically formed [25]. More detailed experimental and theoretical studies were performed in [26], in which the effect of different Co_3O_4 crystal plane orientations was investigated. This study aimed at reducing the charge-discharge overpotential toward an application in high energy density Li-O_2 batteries, and it was established that the (111) surface is the most efficient. Experimentally, the cobalt spinel (110) surface was thoroughly investigated by Petitto and Langell [27] using low-energy electron diffraction (LEED), Auger electron spectroscopy, and x-ray photoelectron spectroscopy. The Co_3O_4(111) surface has been studied using x-ray diffraction (XRD) and atomic force microscopy methods [28], LEED, and scanning tunneling microscopy [29–32]. Bulk Co_3O_4 has also been studied using Raman spectroscopy [33]. In general, Co_3O_4 attracts interest because of its high catalytic activity, especially for CO oxidation [34]; therefore, most of the research has been performed to find such an application. Concerning the theory, a number of publications have been dedicated to *ab initio* study of electronic and magnetic properties of the bulk and surfaces of Co_3O_4 [35–42]. The main problem, discussed in the above-cited theoretical works, is usually the nature of superexchange in bulk spinel and the stability of its surfaces under different conditions, such as different atom types (Co^{2+}, Co^{3+} ions, or O) at the top layer termination.

Another field of cobalt spinel application is related to the interface between *p*-type Co_3O_4 and *n*-type ZnO, which forms a *p*-*n* heterojunction. In particular, *p*-Co_3O_4/*n*-ZnO composites can provide higher sensitivities and faster responses in gas sensor applications [20,34,40,43,44]. Such composites are typically obtained using a mixture of ZnO and Co_3O_4 powders and annealing, which forms an inhomogeneous interface between both semiconductors. However, the presence of this interface also plays a significant role in the magnetic properties of such composites. Indeed, there is evidence of the appearance of magnetism in a ZnO/Co_3O_4 powder mixture at room temperature even without thermal treatment [45,46]. The authors of those studies explained this phenomenon as surface reduction of the Co_3O_4 nanoparticles, in which the antiferromagnetic Co_3O_4 nanoparticle is surrounded by a CoO-like shell. Other authors [47] studying a ZnO/Co_3O_4 powder mixture with x-ray absorption spectroscopy and optical spectroscopy explained such a phenomenon as the reduction $Co^{3+} \rightarrow Co^{2+}$ at the Co_3O_4 nanoparticle surface. This explanation has been proved by vibrating sample magnetometer analysis of composite ZnO, synthesized on the surface of core Co_3O_4 in [48]. Recently, a diode consisting of a *p*-type Co_3O_4 nanoplate/*n*-type ZnO nanorod heteroepitaxal junction was fabricated, showing reasonable electrical performance [49], but no attention has been paid to its magnetic properties. Despite extensive investigation of cobalt oxides, as mentioned above, there is still no clear picture of the role of the cobalt oxide surfaces and interfaces in the magnetic properties.

Considering the lack of microscopic understanding of the surface and interface magnetism, the present study aims to establish the nature of ferromagnetism at the Co_3O_4/ZnO interface toward an application in the new device types for spintronics. We have investigated from first-principles modifications of the atomic structure at various types of Co_3O_4/ZnO boundaries, the related changes in the electronic band structure and their contribution to the appearance of the interface magnetic properties. This paper is organized as follows. We present in Sec. II the numerical formalism used throughout the paper. Section III discusses the microscopic atomic structure of the Co_3O_4(111) surfaces and Co_3O_4/ZnO interfaces. The results for the calculated magnetic and electronic properties and their modifications due to the surfaces or interfaces are discussed in Sec. IV. The conclusion is presented in Sec. V.

II. NUMERICAL METHOD

We investigated the atomic and electronic structure of the Co_3O_4/ZnO interface within the density functional theory (DFT) and generalized gradient approximation (GGA), as implemented in the QUANTUM ESPRESSO software package [50]. We have used ultrasoft Perdew-Burke-Ernzerhof (PBE) pseudopotentials [51], which include 12 valence electrons for zinc, 6 valence electrons for oxygen, and 9 valence electrons for cobalt. An integration of the Brillouin zone was performed using a 4×4 Γ-centered grid of special points in k space, generated by the Monkhorst-Pack scheme [52] and Methfessel-Paxton smearing [53] with a parameter of 0.005 Ry. Several tests were performed with denser grids up to 10×10, but no significant changes were observed compared to the case of the 4×4 grid. To ensure a sufficient convergence of the results we applied a 40-Ry cutoff for the smooth part of the wave function and 400 Ry for the augmented charge density. We approximated the exchange-correlation functional with both the local spin-resolved generalized gradient approximation (SGGA) and the so-called SGGA+U approximation, in which the effect of electron correlations in the 3d shell is taken into account by considering the on-site Coulomb interactions within the Hubbard method [37,54]. We have chosen the value

of the Hubbard U parameters to be 3.5 and 5.0 eV for Co and Zn atoms, respectively.

Although the Hubbard parameters chosen are commonly accepted in the literature, they still are the subject of discussion [37]. Therefore, DFT+U calculations of Co_3O_4 should be carried out with care: the systems under consideration might have several solutions, and there is no guarantee that the lowest-energy solution corresponds to the global minimum. For this reason, we have checked that our conclusions do not depend in a sensitive way on these Coulomb parameters. As discussed in [54], the DFT+U instability can be further exacerbated in the presence of f orbitals and the absence of the gap between the filled and empty states. However, surfaces and interfaces considered here are semiconducting, and the f states are not present. To make sure that the Coulomb parameter choice did affect our results, we followed the established approach from [39]. In particular, (i) we applied a Methfessel-Paxton smearing technique of the Brillouin-zone integration that, as proved, ensures the convergence to the global minimum for both metals and systems with nonzero energy gap. (ii) We also considered several different values of the Hubbard parameter and found that the calculations consistently converge to the same energy.

To optimize the atomic geometry of Co_3O_4 surfaces and Co_3O_4/ZnO interfaces we performed structural relaxations within the SGGA method, and the final calculations of the magnetic structure and the densities of states were carried out using the SGGA+U method. The systems were relaxed through all of the internal coordinates until the Hellmann-Feynman forces became less than 10^{-4} a.u. while keeping the shape and the volume of the supercell fixed.

III. SURFACE AND INTERFACE STRUCTURAL DETAILS

To investigate the origin of the surface/interface magnetism we model two types of $Co_3O_4(111)$ surfaces and two ZnO(0001)/$Co_3O_4(111)$ interfaces. While the above-considered surfaces and interfaces are well suited to numerical simulations, in addition to (111) planes, differently oriented interfaces were observed experimentally [25,43,55–57]. However, as we discuss below, the main magnetic features predicted for the (111) system considered should also be common for differently oriented interfaces in the experimentally observed materials.

The bulk-terminated atomic structure of the $Co_3O_4(111)$ spinel surface in the [111] direction, perpendicular to the surface, can be described by a sequence of atomic layers containing Co^{2+} ions or both Co^{2+} and Co^{3+} ions, separated by a layer of oxygen: O-Co^{2+}-O-$Co^{2+}Co^{3+}$. The primitive unit cell containing such a sequence has hexagonal symmetry along the surface or the interface. The upper layer, which forms the interface with ZnO, contains either three Co^{3+} ions (B-terminated layer) or a combination of two Co^{2+} and one Co^{3+} ions (A-terminated layer; this convention is used since the cobalt oxide layer closest to the interface is type A). The interface between the upper layer of Co_3O_4 and ZnO is then formed by introducing a single layer of four oxygen atoms, which match the Co-O bonds of the spinel. These four oxygen atoms can also be viewed as those belonging to ZnO in the sequence Zn-O-Zn-O in the primitive unit cell: the topology of this spinel oxygen layer has the same symmetry as the (0001) plane of hexagonal ZnO. Hence, to form the epitaxial interface with Co_3O_4 and to saturate these oxygen bonds, four primitive unit cells of hexagonal ZnO are required. In such a way, oxygen atoms play the role of a "bridge" between cubic spinel Co_3O_4 and wurtzite ZnO.

We paid special attention when choosing the lateral unit-cell size of the interface for the systems under investigation since $Co_3O_4(111)$ and ZnO(0001) demonstrate considerable lattice mismatch. To simulate the ZnO(0001)/$Co_3O_4(111)$ interface three possibilities exist: (i) choosing the spinel bulk constant to determine the interface unit-cell size, (ii) using ZnO bulk parameters to define the interface unit cell, and (iii) optimizing the lattice parameter for the interface to find the unit-cell size that minimizes the total energy of the interface. Following the experimental finding, we did not optimize the lattice parameter for the interface since such optimization should lead to both ZnO and Co_3O_4 material being stressed. Indeed, for our case, while such a mismatch should make the epitaxial growth of the flat Co_3O_4/ZnO interface challenging, the experimental microscopic images demonstrate the smooth interface between the Co_3O_4 inclusions and ZnO host material [43,55,57] without a noticeable modification of the interlayer distances and dislocation appearance. Since Co_3O_4 is supposed to be the source of the magnetism, first, we chose the spinel bulk constant as the main structural parameter, resulting in a compressed ZnO part of the system, and then relaxed the atomic positions in the interface vicinity. Considering the experimental value of the bulk spinel lattice constant $a_{\text{spinel}} = 8.084$ Å, a primitive unit cell of its (111) surface has a lattice constant $c_{\text{spinel}} = 5.72$ Å. Since the corresponding parameter of ZnO has a value $c_{\text{ZnO}} = 3.25$ Å, in order to fit four primitive unit cells of ZnO onto a single two-dimensional unit cell of spinel, the bulk constant of ZnO should be compressed in the basal plane by about 12%. Therefore, the lattice constant of this strained ZnO at the interface region is 2.86 Å. As suggested in [49] for ZnO nanorods on Co_3O_4 nanoplates, such a large stress is relieved by forming dislocations along the basal plane at the interface. In the case of the Co_3O_4 inclusions, however, they have low diameters, and the inclusion curvature allows to easily accommodate the strain through the lateral relaxation, thus making heteroepitaxial growth possible even in the case of high lattice mismatch [55]. Additionally, in the present calculations such a stress effect is partially taken into account by the system relaxation within the unit cell. On the other hand, the study of possible extended dislocations that originate due to the mismatch requires simulation of significantly larger unit cells and is out of the scope of our research.

Second, we have chosen to test the ZnO unit-cell size for the interface which resulted in the "stretched" Co_3O_4 side. However, when we carried out the relaxation of the atomic positions in the vicinity of the interface, the spinel-like structure of Co_3O_4 was not preserved. Again, considering the experimental finding of the bulklike Co_3O_4 spinel inclusions in XRD spectra [58], the existence of such stretched Co_3O_4 systems does not look credible. To confirm this conclusion we again compared our theoretical results with the experimental Raman spectra, as discussed below.

Therefore, to study magnetic and electronic structures of an interface, we created two symmetric slabs containing seven

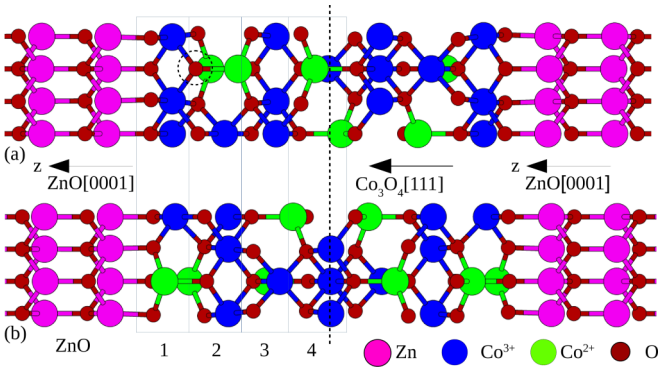

FIG. 1. Side view of the unit cells of Co_3O_4/ZnO interfaces: (a) octahedral B-terminated interface and (b) tetrahedral A-terminated interface. Numbers denote the atomic layers of both interfaces.

atomic layers of Co_3O_4 and ZnO layers adjacent on both sides, as shown in Fig. 1. The first slab [Fig. 1(a)] is composed of a spinel top layer containing Co^{3+} ions at only the B sites ("octahedral" interface), while the second slab [Fig. 1(b)] contains at the interface both Co^{2+} (A-site) and one Co^{3+} (B-site) ions ("tetrahedral" interface). In such a way, each slab contains two interface regions of the same symmetry (topology), so their total dipole moment is close to zero. The ZnO part of the slab is two lattice constants c_{ZnO} thick on both sides, and 12 Å of vacuum layer have been added to separate the slabs in the z direction. Additionally, we have studied the bulk spinel properties using the $12\times12\times12$ k-point grid and its clean (111) surface using the same method. We simulated the Co-terminated and O-terminated spinel (111) surfaces using the slabs created for the interface model but with ZnO layers removed and followed by subsequent relaxation over all coordinates.

IV. RESULTS AND DISCUSSION

We constructed the interface and surface models assuming that the secondary phase preserves bulk spinel crystal structure with the corresponding bulk constant. Our assumption is based on a comparison with the Raman spectra calculated [59] and measured [33,58] for both Co_3O_4 and $Zn_{1-x}Co_xO$. In general, the symmetry of the bulk spinel unit cell is described by point group $\Gamma(O_h^7)$ [60], and therefore, the phonon normal modes near the Brillouin-zone center may be obtained with the decomposition $\Gamma(O_h^7) = A_{1g} + E_g + 3F_{2g} + 5F_{1u} + 2A_{2u} + 2E_u + 2F_{2u}$. Here A_{1g}, E_g, and triply degenerate $3F_{2g}$ modes are Raman active. We calculated the frequencies of these phonon modes for bulk spinel with a lattice constant $a_{spinel} = 8.084$ Å (corresponding to the case of a normal spinel secondary phase and compressed ZnO at the interface) and "stretched" spinel using the experimental ZnO bulk constant, which leads to $a_{spinel} = 9.191$ Å, using density functional perturbation theory [61]. The PBE pseudopotentials were selected in norm-conserving form; the wave-function expansion cutoff of 80 Ry and $4\times4\times4$ k-point grid for Brillouin-zone integration were adopted for these calculations. The calculated and measured Raman frequencies are listed in Table I, which shows that the calculated Raman spectra are very sensitive to the choice of the lattice constant. Frequencies obtained in both local-density approximation (LDA) and GGA approximations for normal spinel are comparable to measured ones, while those calculated for stretched spinel are found to be significantly lower and are not observed experimentally. Moreover, XRD measurements of $Zn_{1-x}Co_xO$ [58] do not indicate the presence of any other structures besides ZnO and $ZnCo_2O_4$. The above comparison of the theoretical and experimental frequencies favors using the bulk Co_3O_4 constant when modeling the interface with ZnO.

TABLE I. Raman-active bulk phonon modes of Co_3O_4(cm^{-1}). The last two rows show the frequencies calculated in this study.

	F_{2g}	E_g	F_{2g}	F_{2g}	A_{1g}
Co_3O_4 [33]	194.4	482.4	521.6	618.4	691.0
$Zn_{1-x}Co_xO$ [58]		486	524	623	710
Co_3O_4 LDA [59]	192	480	511	589	644
Co_3O_4 GGA	187.0	463.9	502.8	574.5	631.7
Stretched Co_3O_4 GGA	62.3	175.4	236.8	325.2	383.8

The calculated lattice constant for bulk spinel $a_{spinel} = 8.147$ Å and the corresponding interplanar A-B spacing $d_{111} = 2.351$ Å are overestimated by only 0.8% compared to the experimental values of $a_{spinel} = 8.084$ Å and $d_{111} = 2.333$ Å, respectively. Therefore, we used the experimental spinel bulk constant.

As mentioned in Sec. III, the unit cell of the spinel (111) plane in the slab construction is hexagonal, and therefore, four unit cells of ZnO (also hexagonal) are needed to match one spinel unit cell. Consequently, the planar lattice constant of adjacent ZnO $a_{ZnO} = 2.88$ Å is scaled to the spinel lattice constant and cannot be optimized separately. However, the interplanar distances (in the z direction) are optimized for both the spinel and the wurtzite regions of the interface. Therefore, the calculated value of the interplanar spacing at the spinel region of the interface becomes $d_{111} = 2.387$ Å, which is about 2% larger than the experimental bulk interplanar distance, while the lattice constant calculated for ZnO regions $c_{ZnO} = 5.52$ Å, which is about 5% above the corresponding experimental bulk value of 5.27 Å. These relaxations absorb part of the stress due to the lattice mismatch between spinel and wurtzite. The optimized supercells of Co_3O_4/ZnO interfaces are shown in Fig. 1. Since there are no dangling bonds at the interfaces and all the ions are located in such a way that the bulk crystalline symmetry is preserved, no significant modifications in the topology of adjacent atomic layers were found during the relaxation. In the case of surfaces, four possibilities exist: B or A termination with a Co or O top layer. The B-terminated sample with Co top layer demonstrates atomic reordering: the oxygen atom of the second layer [the O atom circled by the dashed line in Fig. 1(a)] moves in the z direction to be in the same plane as the Co atoms of first layer. Such reordering occurs in only the Co^{3+}-terminated surface: A-terminated surfaces with both Co and O top layers and a B-terminated surface with an O top layer demonstrate stable surface topology with no significant changes in the overall atomic positions compared to those in the interfaces. We also performed geometry optimization for Co_3O_4 slabs nine atomic

TABLE II. Magnetic moments μ (in units of μ_B) and charges ρ of Co ions (in a.u.), calculated using Löwdin charge analysis, for octahedral surfaces and interfaces.

	Co-terminated surface	O-terminated surface	ZnO interface	Bulk
Co^{3+}				
μ	2.33	0.71	0.21	0.0
ρ	0.94	1.17	1.07	1.02
Co^{2+}				
μ	2.45	2.48	2.46	2.59
ρ	1.16	1.23	1.21	1.22

layers thick and found that the results are practically identical to the case considered in Fig. 1.

We discussed above that in the bulk spinel Co^{3+} ions are nonmagnetic due to the large splitting between t_{2g} and e_g orbitals, caused by the presence of the octahedral crystal field. Since this symmetry is broken at the surface or interface, the electrons could occupy t_{2g} and e_g orbitals in a different order, leading to the changes in magnetic properties reported in [39,47]. It is important to stress that similar symmetry changes are typical for other Co_3O_4 interface orientations; therefore, the results for the $Co_3O_4(111)$ surface, considered here, should reflect general trends in the interface-induced magnetism origin. To quantify these changes, we calculated and compared the magnetic moment of Co ions for different interface and surface systems using a Löwdin charge analysis. Table II shows the largest values of magnetic moments calculated for the bulk Co_3O_4, interfaces, and surfaces, both Co and O terminated. The magnetic moments are calculated for the top layer for Co^{3+} ions and in the second layer of the octahedral interface or surface for Co^{2+} ions. The deviation of the magnetic moment of the same ion type on different sites is relatively small, $\sim 0.02\mu_B$ for all systems, so such values reflect the general physical picture.

The calculated magnetic moment of Co^{2+} ions is slightly smaller in the case of all considered surfaces than in bulk spinel, which has a value of $2.59\mu_B$, as seen from Table II. Instead, while the magnetic moment of Co^{3+} ions is zero in the bulk, it is nonvanishing in the case of the surface. The largest magnetic moment of $2.33\mu_B$ occurs at the Co-terminated surface, where the bulk symmetry is broken and the ion coordination number is reduced the most. If the surface is O terminated, the magnetic moment of Co^{3+} ions reduces to $0.71\mu_B$, while the external oxygen atoms have a magnetic moment of $0.34\mu_B$ due to strong polarization of the p orbitals. The charge calculated for Co^{3+} ions in the bulk is about 0.2 a.u. larger than that of Co^{2+}, as shown in Table II. These values differ slightly for all of the systems under study, and in general, we have to introduce new oxidation state types for Co ions in interfaces and surfaces. However, in our calculations the charge of Co^{3+} is always larger than that of Co^{2+}, and this fact allows us, for the sake of simplicity, to use the explicit "bulk" notations Co^{2+} and Co^{3+} for corresponding ions in all of the systems. The spin density distribution for the tetrahedral interface is shown in Fig. 2. The blue and red regions around the Co^{2+} ions of layers 1 and 3 indicate the presence of magnetic moment, comparable to that in the bulk. Co^{3+} ions in layers

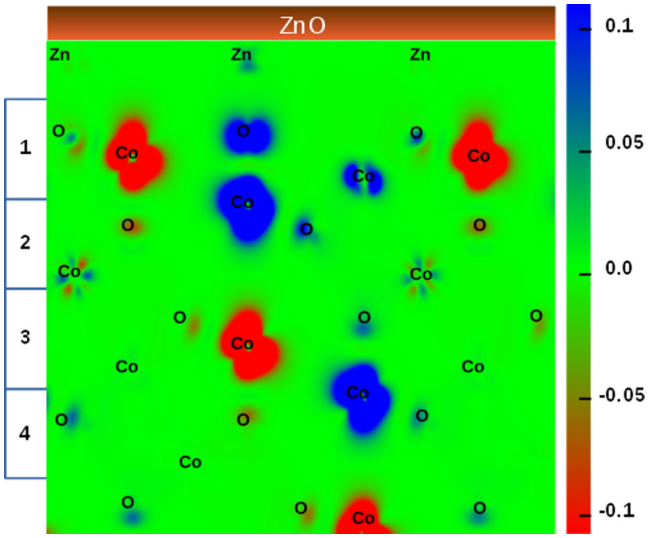

FIG. 2. Spin density distribution for the octahedral interface, plotted over the vertical $(1\bar{1}0)$ plane. The scale, shown on the right, has units of μ_B. On the left, 1, 2, 3, and 4 stand for the Co_3O_4 interface layer numbers. Chemical symbols indicate the positions of corresponding ions.

3 and 4 are completely bare, that is, spin compensated, but have a small magnetic moment in layer 2, which becomes noticeably larger at the interfacing layer. Similar to the case of an O-terminated surface, one of the oxygen ions acquires a magnetic moment of $0.22\mu_B$, as indicated by the blue color. Obviously, such a magnetic ordering corresponds to the AFM state: we calculated the total energy for the different spin orientations, and for this tetrahedral interface the difference between the energies of the ferromagnetic (FM) and AFM states is $E_{FM} - E_{AFM} = 94$ meV. For the octahedral interface the FM state is energetically preferable, and the difference in energy between the FM and AFM states is -23 meV. In general, the lowest total energy is found for the octahedral interface with FM magnetic ordering.

A more accurate method to estimate the relation between the interface type and magnetic ordering is to calculate the formation energy. Such an approach, however, requires knowledge of the chemical potentials of the ions involved. To the best of our knowledge, this problem has not been solved yet: the main challenge is to properly find these potentials for ions in different oxidation states.

It is worth noting that the magnetic moments were calculated for the relaxed systems while keeping the C_{3v} symmetry intact. If this symmetry is broken (for instance, for differently oriented interfaces or when the initial deviations from equilibrium positions are different for symmetry-equivalent atoms or due to defects), the corresponding magnetic moments might differ slightly. Nevertheless, the general picture should remain the same: Co^{3+} ions gain nonzero magnetic moments at both the surface and interface, in contrast to the bulk case. Therefore, the magnetic effects discussed above should also be present for differently oriented parts of the Co_3O_4 inclusions.

As is already known, the presence of dangling bonds leads to additional surface states observable in the density of states (DOS). The formation of the interface between two different materials is also responsible for the interface states, localized

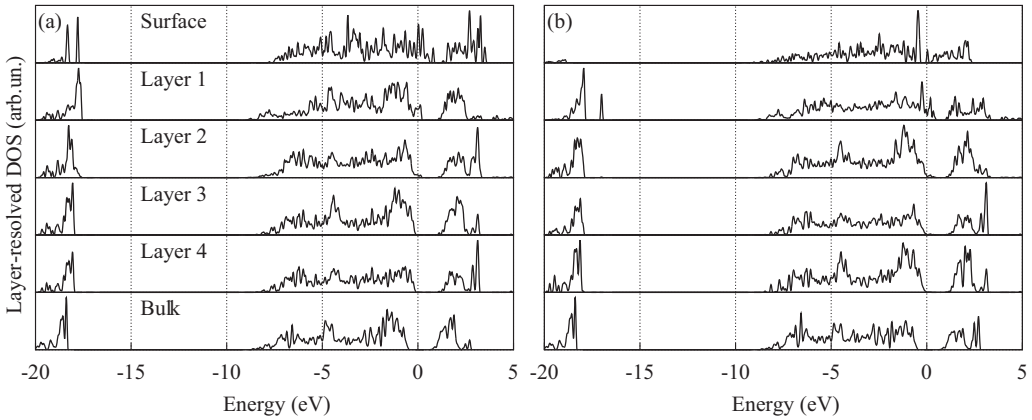

FIG. 3. Layer-resolved DOS of (a) octahedral and (b) tetrahedral spinel (111) surfaces and (111) spinel/(0001) wurtzite interfaces. From top to bottom: top layer of spinel (111) surface with no ZnO cap, layers 1 to 4 of the spinel structure close to the spinel/wurtzite interface, and the layer-resolved DOS for the (111) plane of bulk spinel (see discussions in the text).

close to the boundary between the two materials. The surface or interface formation causes the charge redistribution and change in the corresponding magnetic properties. To demonstrate this we first calculated the spin-averaged layer-resolved DOS (LRDOS) for all systems under investigation, as shown in Fig. 3. For the bulk spinel, the planes that pass through the Co ions of the corresponding charge state (A or B type) were used as in the LRDOS calculations. All LRDOSs there are aligned in such a way that the highest filled states (Fermi level) are at zero energy. For the top layer of Co-terminated surfaces, there is clear evidence of such surface states present in the DOS (top panels in Fig. 3, denoted "surface"). It contains a lot of features not present in the bulk, and such a picture, in principle, is typical for all the considered surfaces with dangling bonds. There is a notable difference in Co-terminated surface DOSs for octahedral and tetrahedral terminations in the region of -18 eV due to the oxygen atom shifting from layer 2 to the top layer of the octahedral system. On the other hand, in the tetrahedral system the top layer consists of only Co atoms. The LRDOS of O-terminated surfaces (not shown) demonstrates no noticeable difference from the Co-terminated surface for both tetrahedral and octahedral coordinations. In this case, for both coordinations, the bonds of surface Co atoms now are passivated by oxygen atoms and are no longer broken. This means that there are also other factors responsible for the formation of the inside band-gap states. Such a situation is also observed in the case of the interface. One can see from Fig. 3 (panels denoted "layer n," with $n = 1$, 2, 3, and 4) that LRDOS for the first layer demonstrates surfacelike states inside the band gap close to the top of the valence band. For the internal layers these surfacelike states decay with depth, almost disappearing at layer 4. The corresponding LRDOS becomes bulklike for both octahedral and tetrahedral coordinations, as seen from the comparison between the LRDOSs of layer 4 and those denoted "bulk" in Fig. 3.

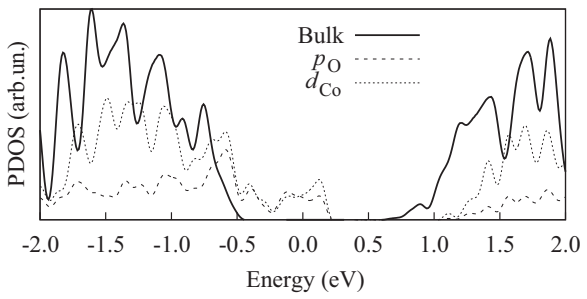

FIG. 4. Projected LRDOS for the top layer of the octahedral interface and octahedral plane of bulk spinel. The plot demonstrates the dominance of the p and d components of the wave function, while the s-state contributions can be neglected.

Comparing LRDOSs calculated for the surface and interface, one can conclude that although each Co ion at the interface layer keeps the symmetry of the bulk crystalline environment, the physical properties of the interface region are closer to those of the surface than to those of the bulk. To understand the origin of the surfacelike states in the band gap, we calculated the LRDOS of the octahedral interface, projected onto atomic wave functions of a corresponding Co atom (s and d orbitals) and O atom (s and p orbitals), localized at the octahedral interface, as shown in Fig. 4. For convenience, we also plotted the LRDOS for the A plane of bulk spinel. As can be seen, surfacelike states originate predominantly from O $2p$ states and Co $3d$ states, while the contribution of s states of both Co and O is negligibly small here. Similar conclusions about the origin of the surface states in the tetrahedral systems have also been obtained. From this we conclude that the charge state of the Co ion is not decisive in defining the surface or interface magnetism since in both cases p orbitals of the O atoms make the same contribution to the DOS. Moreover, from the band structure calculation we see that the partially occupied states are common for all of the surfaces and interfaces under investigation. This demonstrates the metal-like electronic structure, in contrast to the bulk spinel, which appears to be semiconducting in the simulations even when larger smearing parameters in the Brillouin-zone integration are used.

V. CONCLUSION

We investigated the origin of the surface/interface magnetism of the Co_3O_4 surfaces and their interfaces with

ZnO. In particular, we studied the structural, electronic, and magnetic properties using model systems such as ZnO(0001)/Co_3O_4(111) interfaces, Co_3O_4(111) surfaces for A-type and B-type terminations, and bulk spinel. We showed that while the magnetic moment of Co^{3+} ions is zero in the bulk, it does not vanish at the interface or surface, where its value becomes comparable with the magnetic moment of Co^{2+} due to the created imbalance in the electron distribution. The calculated LRDOS demonstrates that although Co ions at the interface have the same neighboring atoms as in bulk spinel, their DOS exhibits a surfacelike nature, arising from polarized Co 3*d* and O 2*p* orbitals of the interfacing layer. In all cases, interface or surface and A- or B-type termination, we observed metalliclike states, localized at the surface or interface, which are responsible for the surface/interface magnetism. Whereas the magnetic order is antiferromagnetic in the bulk spinel at low temperature, the metallic surface/interface states indicate the possibility of ferromagnetic order at the surfaces or interfaces. The proposed mechanisms offer a possible interpretation of the experimental observation of the net magnetic moment in Co-doped ZnO with high Co concentrations.

ACKNOWLEDGMENTS

We thank O. Kolomys and V. Strelchuk for useful discussions. This work was supported by NATO (Grant No. NUKR.SFPP 984735). I.M.K. acknowledges EC for the H2020 MSCA RISE project CoExAN (GA 644076). The CPU time was provided by the Shared Hierarchical Academic Research Computing Network (Sharcnet) of Ontario, Canada.

[1] F. Matsukura, H. Ohno, A. Shen, and Y. Sugawara, Phys. Rev. B **57**, R2037 (1998).
[2] K. Olejník, M. H. S. Owen, V. Novák, J. Mašek, A. C. Irvine, J. Wunderlich, and T. Jungwirth, Phys. Rev. B **78**, 054403 (2008).
[3] T. Dietl, H. Ohno, F. Matsukura, J. Cibert, and D. Ferrand, Science **287**, 1019 (2000).
[4] H.-J. Lee, S.-Y. Jeong, C. R. Cho, and C. H. Park, Appl. Phys. Lett. **81**, 4020 (2002).
[5] K. Sato and H. Katayama-Yoshida, Jpn. J. Appl. Phys. **40**, L334 (2001).
[6] P. Sati, R. Hayn, R. Kuzian, S. Régnier, S. Schäfer, A. Stepanov, C. Morhain, C. Deparis, M. Laügt, M. Goiran, and Z. Golacki, Phys. Rev. Lett. **96**, 017203 (2006).
[7] S. Stefanowicz, G. Kunert, C. Simserides, J. A. Majewski, W. Stefanowicz, C. Kruse, S. Figge, T. Li, R. Jakieła, K. N. Trohidou, A. Bonanni, D. Hommel, M. Sawicki, and T. Dietl, Phys. Rev. B **88**, 081201 (2013).
[8] G. D. Nipan, V. A. Ketsko, T. N. Kol'tsova, A. I. Stognii, K. I. Yanushkevich, V. V. Pan'kov, A. M. Khoviv, and A. M. Solodukha, Russ. J. Inorg. Chem. **51**, 1961 (2006).
[9] Y. Wang, S. Yuan, Y. Song, L. Liu, Z. Tian, P. Li, Y. Zhou, Y. Li, and S. Yin, Chin. Sci. Bull. **52**, 1019 (2007).
[10] J.-j. Li, W.-c. Hao, H.-z. Xu, and T.-m. Wang, J. Appl. Phys. **105**, 053907 (2009).
[11] H. Çolak and O. Türkoğlu, J. Mater. Sci. Mater. Electron. **26**, 10141 (2015).
[12] T. Dietl, T. Andrearczyk, A. Lipińska, M. Kiecana, M. Tay, and Y. Wu, Phys. Rev. B **76**, 155312 (2007).
[13] T. Dietl, K. Sato, T. Fukushima, A. Bonanni, M. Jamet, A. Barski, S. Kuroda, M. Tanaka, P. N. Hai, and H. Katayama-Yoshida, Rev. Mod. Phys. **87**, 1311 (2015).
[14] R. O. Kuzian, J. Richter, M. D. Kuz'min, and R. Hayn, Phys. Rev. B **93**, 214433 (2016).
[15] X. Wang, J. Xu, X. Yu, K. Xue, J. Yu, and X. Zhao, Appl. Phys. Lett. **91**, 031908 (2007).
[16] A. Walsh, S.-H. Wei, Y. Yan, M. M. Al-Jassim, J. A. Turner, M. Woodhouse, and B. A. Parkinson, Phys. Rev. B **76**, 165119 (2007).
[17] Y. Sharma, N. Sharma, G. V. Subba Rao, and B. V. R. Chowdari, Adv. Funct. Mater. **17**, 2855 (2007).
[18] M. Bajdich, M. García-Mota, A. Vojvodic, J. K. Nørskov, and A. T. Bell, J. Am. Chem. Soc. **135**, 13521 (2013).
[19] H.-J. Kim and J.-H. Lee, Sens. Actuators B **192**, 607 (2014).
[20] D. R. Miller, S. A. Akbar, and P. A. Morris, Sens. Actuators B **204**, 250 (2014).
[21] *Oxide Materials at the Two-Dimensional Limit*, edited by F. P. Netzer and A. Fortunelli, Springer Series in Materials Science, Vol. 234 (Springer, Cham, 2016).
[22] W. Roth, J. Phys. Chem. Solids **25**, 1 (1964).
[23] C. E. Rodríguez Torres, F. Golmar, M. Ziese, P. Esquinazi, and S. P. Heluani, Phys. Rev. B **84**, 064404 (2011).
[24] J. Noh, O. I. Osman, S. G. Aziz, P. Winget, and J.-L. Brédas, Chem. Mater. **27**, 5856 (2015).
[25] J. Hutchison and N. Briscoe, Ultramicroscopy **18**, 435 (1985).
[26] D. Su, S. Dou, and G. Wang, Sci. Rep. **4**, 5767 (2014).
[27] S. C. Petitto and M. A. Langell, J. Vac. Sci. Technol. A **22**, 1690 (2004).
[28] J. Buršík, M. Soroka, R. Kužel, and F. Mika, J. Solid State Chem. **227**, 17 (2015).
[29] P. Thurian, G. Kaczmarczyk, H. Siegle, R. Heitz, A. Hoffmann, I. Broser, B. Meyer, R. Hoffbauer, and U. Scherz, in *Proceedings of the 18th International Conference on Defects in Semiconductors: ICDS-18, Sendai, Japan*, edited by M. Suezawa and H. Katayama-Yoshida, Materials Science Forum (Trans Tech Publications, Zurich, Switzerland, 1995), Vols. 196–201, pp. 1571–1576.
[30] P. Ferstl, S. Mehl, M. A. Arman, M. Schuler, A. Toghan, B. Laszlo, Y. Lykhach, O. Brummel, E. Lundgren, J. Knudsen, L. Hammer, M. A. Schneider, and J. Libuda, J. Phys. Chem. C **119**, 16688 (2015).
[31] C. Vaz, V. Henrich, C. Ahn, and E. Altman, J. Cryst. Growth **311**, 2648 (2009).
[32] S. Mehl, P. Ferstl, M. Schuler, A. Toghan, O. Brummel, L. Hammer, M. A. Schneider, and J. Libuda, Phys. Chem. Chem. Phys. **17**, 23538 (2015).
[33] V. G. Hadjiev, M. N. Iliev, and I. V. Vergilov, J. Phys. C **21**, L199 (1988).
[34] D. Bekermann, A. Gasparotto, D. Barreca, C. Maccato, E. Comini, C. Sada, G. Sberveglieri, A. Devi, and R. A. Fischer, ACS Appl. Mater. Interf. **4**, 928 (2012).
[35] A. Montoya and B. S. Haynes, Chem. Phys. Lett. **502**, 63 (2011).
[36] J. Chen and A. Selloni, J. Phys. Chem. Lett. **3**, 2808 (2012).
[37] S. Selcuk and A. Selloni, J. Phys. Chem. C **119**, 9973 (2015).
[38] M. Wang and Q. Chen, Chem. Eur. J. **16**, 12088 (2010).

[39] J. Chen and A. Selloni, Phys. Rev. B **85**, 085306 (2012).
[40] X.-L. Xu, Z.-H. Chen, Y. Li, W.-K. Chen, and J.-Q. Li, Surf. Sci. **603**, 653 (2009).
[41] F. Zasada, W. Piskorz, and Z. Sojka, J. Phys. Chem. C **119**, 19180 (2015).
[42] I. Kupchak and N. Serpak, Ukr. J. Phys. **62**, 615 (2017).
[43] T. K. Jana, A. Pal, and K. Chatterjee, J. Alloys Compd. **653**, 338 (2015).
[44] S. Park, S. Kim, H. Kheel, and C. Lee, Sens. Actuators B **222**, 1193 (2015).
[45] M. S. Martín-González, M. A. García, I. Lorite, J. L. Costa-Krámer, F. Rubio-Marcos, N. Carmona, and J. F. Fernández, J. Electrochem. Soc. **157**, E31 (2010).
[46] A. Quesada, M. A. García, M. Andrés, A. Hernando, J. F. Fernández, A. C. Caballero, M. S. Martín-González, and F. Briones, J. Appl. Phys. **100**, 113909 (2006).
[47] M. A. García, F. Jiménez-Villacorta, A. Quesada, J. de la Venta, N. Carmona, I. Lorite, J. Llopis, and J. F. Fernández, J. Appl. Phys. **107**, 043906 (2010).
[48] S. A. Kulkarni, P. S. Sawadh, and P. K. Palei, J. Korean Chem. Soc. **58**, 100 (2014).
[49] T. I. Lee, S. H. Lee, Y.-D. Kim, W. S. Jang, J. Y. Oh, H. B. Koo, C. Stampfl, A. Soon, and J. M. Myoung, Nano Lett. **12**, 68 (2012).
[50] P. Giannozzi, S. Baroni, N. Bonini, M. Calandra, R. Car, C. Cavazzoni, D. Ceresoli, G. L. Chiarotti, M. Cococcioni, I. Dabo, A. D. Corso, S. de Gironcoli, S. Fabris, G. Fratesi, R. Gebauer, U. Gerstmann, C. Gougoussis, A. Kokalj, M. Lazzeri, L. Martin-Samos, N. Marzari, F. Mauri, R. Mazzarello, S. Paolini, A. Pasquarello, L. Paulatto, C. Sbraccia, S. Scandolo, G. Sclauzero, A. P. Seitsonen, A. Smogunov, P. Umari, and R. M. Wentzcovitch, J. Phys.: Condens. Matter **21**, 395502 (2009).
[51] J. P. Perdew, K. Burke, and M. Ernzerhof, Phys. Rev. Lett. **77**, 3865 (1996).
[52] J. D. Pack and H. J. Monkhorst, Phys. Rev. B **16**, 1748 (1977).
[53] M. Methfessel and A. T. Paxton, Phys. Rev. B **40**, 3616 (1989).
[54] B. Dorado, G. Jomard, M. Freyss, and M. Bertolus, Phys. Rev. B **82**, 035114 (2010).
[55] D. Bekermann, A. Gasparotto, D. Barreca, C. Maccato, M. Rossi, R. Matassa, I. Cianchetta, S. Orlanducci, M. Kete, and U. L. Štangar, Cryst. Growth Des. **12**, 5118 (2012).
[56] X. Xie, Y. Li, Z.-Q. Liu, M. Haruta, and W. Shen, Nature (London) **458**, 746 (2009).
[57] Y. Liu, G. Zhu, J. Chen, H. Xu, X. Shen, and A. Yuan, Appl. Surf. Sci. **265**, 379 (2013).
[58] T.-L. Phan, N. Nghia, and S. Yu, Solid State Commun. **152**, 2087 (2012).
[59] A. Mock, R. Korlacki, C. Briley, D. Sekora, T. Hofmann, P. Wilson, A. Sinitskii, E. Schubert, and M. Schubert, Appl. Phys. Lett. **108**, 051905 (2016).
[60] D. L. Rousseau, R. P. Bauman, and S. P. S. Porto, J. Raman Spectrosc. **10**, 253 (1981).
[61] S. Baroni, S. de Gironcoli, A. Dal Corso, and P. Giannozzi, Rev. Mod. Phys. **73**, 515 (2001).